Mem. S.A.It. Suppl. Vol. 19, 294

Memorie della
Supplementi

Multi-wavelength strong lensing analyses of baryons and dark matter in galaxy clusters

M. Sereno[1,2], M. Lubini[3], and Ph. Jetzer[3]

[1] Dipartimento di Fisica, Politecnico di Torino, Corso Duca degli Abruzzi 24, 10129 Torino, Italia
[2] INFN, Sezione di Torino, Via Pietro Giuria 1, 10125, Torino, Italia
[3] Institut für Theoretische Physik, Universität Zürich, Winterthurerstrasse 190, 8057 Zürich, Switzerland

Abstract. Strong lensing studies can provide detailed mass maps of the inner regions even in dynamically active galaxy clusters. Proper modelling of the intracluster medium can play an important role. We discuss a parametric method which exploits X-ray and optical observations. The mass model accounts separately for cluster-sized dark matter halos, galaxies and the intracluster medium. This gives an unbiased look at each matter component. The method has been applied to AC 114, an irregular X-ray cluster. The dark matter distribution is shifted and rotated with respect to the gas but follows the galaxy density, which hints at its collisionless nature. Despite the dynamical activity, the matter distribution seems to be in agreement with predictions from N-body simulations. A universal cusped profile provides a good description of either the overall or the dark matter distribution and the cluster is not affected by the lensing over-concentration bias, as further stressed by an analysis of the triaxial structure.

Key words. galaxies: clusters: general – individual: AC 114 – X-rays: galaxies: clusters – cosmology: observations – distance scale – gravitational lensing

1. Introduction

Formation and evolution of galaxy clusters is an open topic in modern astronomy. On the theoretical side, *N*-body simulations make detailed statistical predictions on dark matter (DM) halo properties (Navarro et al. 1997). On the observational side, multiwavelength observations of galaxy clusters, from the radio to the optical bands to X-ray observations, can provide deep insight into real features (Clowe et al. 2004; De Filippis et al. 2005; Smith et al. 2005; Sereno et al. 2006). Results are impressive on both sides, but additional work is still required. Large numerical simulations still cannot efficiently incorporate gas physics, whereas combining multiwavelength data sets can be misleading if the employed hypotheses (hydrostatic and/or dynamical equilibrium, spherical symmetry) do not hold. Areas of disagreement between predictions and measurements therefore persist.

We consider a way of exploiting multi-wavelength data sets in strong lensing data analyses. Strong lensing modelling can give detailed maps of the inner regions of galaxy

Send offprint requests to: mauro.sereno@polito.it

clusters without relying on hypotheses about equilibrium and is negligibly affected by projection effects caused by large-scale fields or aligned structures. Here, we report recent results in Sereno et al. (2010a,b) which introduced a novel approach. A parametric lensing analysis was proposed with three kinds of component: cluster-sized dark matter halos; galaxy-sized (dark plus stellar) matter halos; and cluster-sized gas distribution. In our approach, the intra-cluster medium (ICM) distribution is embedded in the strong lensing modelling from the very beginning to avoid unpleasant biases. To reduce the total number of parameters, the X-ray surface brightness data are fully exploited so that the gas contribution is fixed within the observational uncertainties.

We applied the method to the cluster AC 114, a prototypical example of the Butcher-Oemler effect at redshift $z = 0.315$ (Couch et al. 1998). AC 114 exhibits significant evidence of being an ongoing merging. X-ray morphology is strongly irregular with a main core plus an extended off-centred south-east tail (De Filippis et al. 2004). Many multiple image systems have been detected in the cluster core (Smail et al. 1991; Campusano et al. 2001). For our strong lensing model, we exploited only the image systems with confirmed spectroscopic redshift, i.e., systems A (5 images at $z_s = 1.691$), E (5 images at $z_s = 3.347$), and S (3 images at $z_s = 1.867$).

2. The method

We performed a strong lensing analysis exploiting optical observations, and measurements in the X-ray band. This multiwavelength approach allowed us to model the three main components: the cluster-sized dark matter halo, the cluster-sized ICM, and the observed galaxies. Each component was described with a separate parametric mass model. *i*) To model the cluster-sized DM component, we considered a Navarro-Frenk-White (NFW) density profile. *ii*) The two gas components, i.e., the main X-ray clump and the soft tail, were modelled as β-profiles. A priori information on the gas mass was inferred from the X-ray analysis. *iii*) We also considered the mass distribution of the galaxies in the region of the cluster where the multiple image systems are located. Galaxy-sized halos were modelled as pseudo-Jaffe mass profiles. On the other hand, the baryonic contribution of stars and stellar remnants was estimated independently of lensing by converting galaxy luminosities into stellar masses.

This approach allowed us to constrain the mass model using X-ray data without relying on the assumption of hydrostatic equilibrium. As far as the stellar component is concerned, we followed the usual approach: total galaxy masses (DM plus baryons) were derived using the lensing fitting procedure, whereas the stellar contribution was inferred from luminosity. The main advantage of this approach is that we directly inferred the dark matter mass, i.e., the component most accurately constrained in numerical simulations, so that our novel approach aids the comparison with their theoretical predictions. Furthermore, we could compare the gas distribution with the dark matter, which is an obvious improvement to the usual way of comparing total projected mass distributions with surface brightness maps.

3. Discussion

The strong lensing analysis of the inner regions of AC 114 provided additional insight into its dynamical status. The mass density profile for each component in plotted in Fig. 1. The gas was found to be systematically displaced from the dark matter. The main X-ray clump and the cluster-sized DM halo are off-centre by $\sim 9''$, an offset much larger than the Chandra accuracy of $\sim 1''$. The relative orientation differs by (27 ± 4) deg. On the other hand, the DM clump is nearly aligned with the X-ray tail. This implies that the X-ray surface brightness of the core has been strongly perturbed by the dynamical activity. While the ICM is clearly displaced from the galaxy density, the dark matter distribution follows it. In fact, galaxy and dark matter distributions have comparable centroid positions, orientations, and ellipticities. The agreement provides additional evidence of the collisionless nature of dark matter.

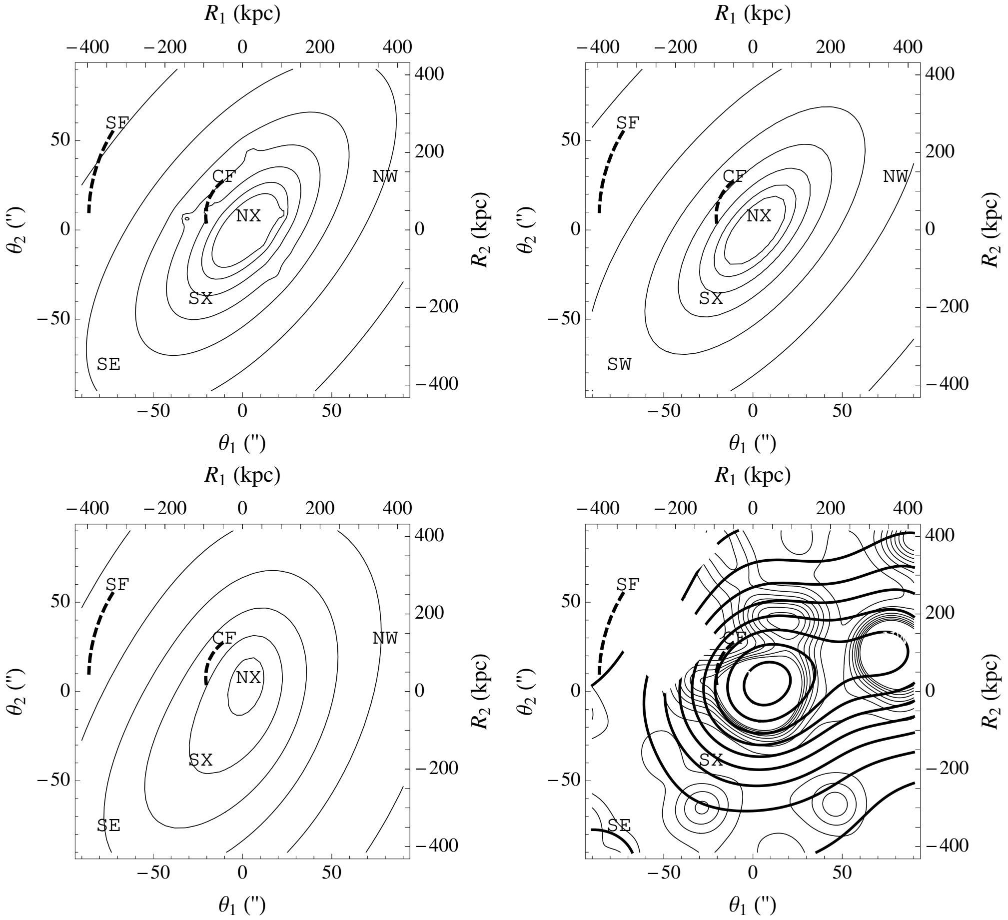

Fig. 1. Surface matter density distribution in the core region of AC 114, in units of the projected critical density for a source redshit at $z_s = 3.347$, $\Sigma_{cr} = 2154.2 M_{\odot}\mathrm{pc}^{-2}$ ($h = 0.7$). Contours represent linearly spaced values of the convergence κ. NW and SE denote the positions of two galaxy clumps; NX and SX mark the location of the X-ray surface brightness peak for the main clump and the tail, respectively. The cold front CF and the shock front SF are plotted as dashed lines. *Top-left*: Contour plot of the total matter density as inferred from lensing. κ-contours are plotted from 0.1 to 0.8 in steps of $\Delta\kappa = 0.1$. *Top-right*: contours of the cluster-sized dark matter halo density as derived from the lensing analysis. κ-contour values go from 0.1 to 0.7 in steps of $\Delta\kappa = 0.1$. *Bottom-left*: projected gas mass density derived from X-ray observations. The convergence contours run from 0.07 to 0.12 in steps of $\Delta\kappa = 0.01$. *Bottom-right*: map of the projected mass density in stars derived from galaxy luminosities. The thick (thin) contours were obtained by smoothing the stellar mass density with a Gaussian kernel of dispersion 30″ (10″). κ-values run from 0.2×10^{-2} to 1.8×10^{-2} in steps of 0.2×10^{-2} for the thick contours and from 2.5×10^{-3} to 2.0×10^{-2} in steps of 2×10^{-3} for the thin contours. From Sereno et al. (2010b).

The baryonic components were mainly constrained using observations either in the X-ray or optical band, allowing us to infer directly the dark matter distribution from the lensing analysis. The mass profile of each component was constrained in the very inner regions. We found typical trends (Biviano & Salucci 2006). The dark matter halo is the most prominent

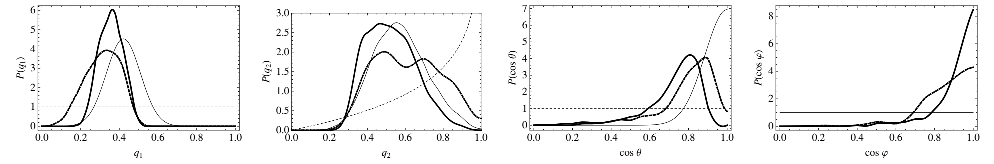

Fig. 2. Posterior probability density functions (PDFs) for the intrinsic parameters. Panels from the left to the right are for the PDF of the intrinsic axial ratio q_1, q_2 and the orientation angles $\cos\theta$ and $\cos\varphi$, respectively. Full and dashed thick lines have been obtained assuming a N-body-like and a flat prior on the axis ratios, respectively. The full and dashed thin line in the left panel represent the N-body and the flat prior for $P(q_1)$, respectively; the full and dashed thin line in the q_2-panel represent the prior distributions according to either a N-body or a flat prior, respectively; the thin and dashed full line in the $\cos\theta$-panel represent the biased and the flat distributions on the orientation angle. The flat line in the $\cos\varphi$-panel represents an uniform distribution. From Sereno et al. (2010a).

component. At the centre ($\lesssim 50$ kpc), the baryonic budget is dominated by the stellar mass of the BCG, whereas the ICM contribution is more important at larger radii. The gas distribution is shallower than the dark matter profile. This picture is compatible with typical values inferred from X-ray analyses of luminous clusters (Allen et al. 2008).

To investigate the inner slope, we considered a total matter distribution modelled as a power law mass profile, i.e., $\rho \propto r^{-\alpha}$. For the slope we obtained a best-fit model value of $\alpha = 1.4 \pm 0.2$, which is steeper than a simple NFW profile and falls just in the middle of the range compatible with theoretical predictions (Diemand et al. 2004).

The concentration parameter depends on the central density of the halo, uncovering imprints of the halo assembly history and thereby of its time of formation. We estimated M_{200} and c_{200} from the projected NFW parameters directly inferred from the fit. We obtained $c_{200} = 3.5 \pm 0.7$, and $M_{200} = (1.3 \pm 0.9) \times 10^{15} M_{\odot}/h$, slightly lower than the mass from the virial theorem.

Intrinsic parameters can be estimated as well assuming a given mass-concentration relation. The three-dimensional structure was modelled as a single ellipsoidal halo. We found the intrinsic shape and orientation which are compatible with the inferred elongation and the measured projected ellipticity. Results for AC 114 support expectations of N-body simulations which prefer mildly triaxial lensing clusters with a strong orientation bias, see Fig. 2.

References

Allen, S. W., Rapetti, D. A., Schmidt, R. W., et al. 2008, MNRAS, 383, 879

Biviano, A. & Salucci, P. 2006, A&A, 452, 75

Campusano, L. E., Pelló, R., Kneib, J.-P., et al. 2001, A&A, 378, 394

Clowe, D., Gonzalez, A., & Markevitch, M. 2004, ApJ, 604, 596

Couch, W. J., Barger, A. J., Smail, I., Ellis, R. S., & Sharples, R. M. 1998, ApJ, 497, 188

De Filippis, E., Bautz, M. W., Sereno, M., & Garmire, G. P. 2004, ApJ, 611, 164

De Filippis, E., Sereno, M., Bautz, M. W., & Longo, G. 2005, ApJ, 625, 108

Diemand, J., Moore, B., & Stadel, J. 2004, MNRAS, 353, 624

Navarro, J. F., Frenk, C. S., & White, S. D. M. 1997, ApJ, 490, 493

Sereno, M., De Filippis, E., Longo, G., & Bautz, M. W. 2006, ApJ, 645, 170

Sereno, M., Jetzer, P., & Lubini, M. 2010a, MNRAS, 403, 2077

Sereno, M., Lubini, M., & Jetzer, P. 2010b, A&A, 518, A55

Smail, I., Ellis, R. S., Fitchett, M. J., et al. 1991, MNRAS, 252, 19

Smith, G. P., Kneib, J.-P., Smail, I., et al. 2005, MNRAS, 359, 417